ORIGINAL RESEARCH

Contact electrification property controlled by amino modification of cellulose fibers

**Zhang Sheng · Zhu Qiuxiao · Wang Tingting ·
Wang Xuchong · Sun Xiaoping · Wei Yuhe ·
Luo Lianxin**

Abstract As a green material, cellulose is widely used in friction triboelectric nanogenerators (TENGs). However, the weak polarity of the cellulose fibers surface leads to its weak contact electrification performance, which is not conducive to its utilization in TENGs. In this study, epoxy chloropropane and ethylenediamine were grafted onto cellulose fibers to form paper and were assembled with an Fluorinated ethylene propylene film. The output voltage, current, and surface charge density were 34.9%, 26.7%, and 16.7% higher than those of ordinary paper, respectively. When 20% nano TiO_2 filler was added to the paper made from amino-modified cellulose fibers, the output voltage, current, and surface charge density of the TENG increased by 70.9%, 226.7%, and 122.2%, respectively, compared with ordinary paper. As the air humidity of the TENG increased from 60 to 90%, the output voltage, current, and surface charge density were maintained at 53.7%, 38.9%, and 61.0%, respectively. When a 5×10^7 Ω resistor was connected to the working circuit, its output power reached 13.78 µ W cm^2. This showed that cellulose as a green material has wide application prospects in the field of TENG.

Z. Sheng · Z. Qiuxiao · W. Tingting · W. Xuchong ·
S. Xiaoping · W. Yuhe · L. Lianxin (✉)
College of Light Industry and Food Engineering, Guangxi University, Nanning 530004, China
e-mail: luolianxin@gxu.edu.cn

Z. Sheng · Z. Qiuxiao · W. Tingting · W. Xuchong ·
S. Xiaoping · W. Yuhe · L. Lianxin
Guangxi Key Laboratory of Clean Pulp & Papermaking and Pollution Control, Guangxi University,
Nanning 530004, China

Introduction

A triboelectric nanogenerator (TENG) is an effective method for obtaining environmental mechanical energy. In 2012, Wang first proposed the concept of a TENG and realized the effective harnessing and conversion of triboelectric power. To date, TENGs have been widely studied (Niu et al. 2013; Wang & Wu, 2012; Zhu et al. 2013). The cathode materials commonly used in TENG friction layers mainly include metals, metal oxides, and polyamides (Yang et al. 2013; Yilin et al. 2019; Zhao et al. 2016). However, metal materials are easily oxidized or corroded under harsh environmental conditions, and this affects the operational stability of TENG systems. Furthermore, most synthetic polymers are nonrenewable and nonbiodegradable. The long-term use of such triboelectric materials can easily cause environmental problems, such as white pollution (Ma et al. 2018; Niu & Wang, 2015; Wu et al. 2019). Therefore, the introduction of new environmentally friendly materials is a new trend for TENGs in the future. The development of green

friction electrode materials is challenging to optimize their performance.

In recent years, natural fiber materials, paper-based materials, and materials derived from lignocellulose fibers have been increasingly used to prepare TENGs (Lai et al. 2019; Wu et al. 2016). Zhang coated a layer of indium tin oxide (ITO) on commercial printing paper to make ITO paper and FET film, which were used to assemble TENG. The short-circuit current density reportedly reached 2.0 mA/m^2 (Zhang et al. 2014). Xia used paper as an electrode substrate and polytetrafluoroethylene (PTFE) tape to prepare a paper-based TENG, working in sliding mode through origami technology. The corresponding maximum open circuit voltage was observed to have reached nearly 1000 V (Xia et al. 2018). However, according to the research of Diaz (2004), the existence of oxygen atoms made cellulose show a high trend of electron loss, which would limit the output performance of paper-based TENG. Therefore, on the one hand, specific functional groups could be introduced into cellulose molecules (Wang et al. 2016), on the other hand, the phonon/electron transport mode of cellulose could be changed through composite fillers to further improve the output performance of paper-based TENG (Fan et al. 2012).

The output performance of the TENG was related to the surface charge density of the friction materials, and the surface charge density was, in turn, related to the difficulty of gaining and losing electrons from friction materials. The easier it is for the materials to gain and lose electrons, the greater the surface charge density (He et al. 2015). Cellulose has an almost neutral relative polarity based on its chemical molecular formula and is in a positive position in the triboelectric material series (Zhu et al. 2016; Zi et al. 2016) and FEP films have strong negative charge (Liu et al. 2020). The weak polarization of natural cellulose leads to its limited ability to generate surface charge, and this makes its performance much lower than that of synthetic polymers. At present, research on improving the properties of lignocellulose-based TENGs has mainly focused on improving the surface charge density by changing the material composition and increasing the effective contact area.

Based on the good chemical modification of lignocellulose fibers (Roy et al. 2009), the friction polarity was enhanced by changing the functional groups on the surface of lignocellulose fiber materials, such as

introducing different functional groups (such as nitro, amino, and methyl) to improve its charge capture ability (Mi et al. 2018a; Yao et al. 2017). The green environmental protection of cellulose fibers was reflected in its degradability. Generally speaking, the other principle introduced into cellulose fibers was the substitution reaction with "–OH" on cellulose fibers. The degradation of cellulose fibers was a reaction in which the functional groups of cellulose fibers were transformed under the action of chemical or physical factors, the degree of polymerization decreased, and caused the breakage of "C–C" bond and "C–O" bond in glucose group, that is, glucoside bond, until it is completely cracked and transformed to produce various small molecular compounds. Therefore, after the introduction of other functional groups, cellulose fibers was still a green environmental protection material. Mi prepared polyethyleneimine-modified cellulose nanofiber (CNF) to prepare aerogels, which not only enhanced the mechanical properties of CNF/PEI aerogels, but also increased the power density by 14.4 times due to the increase in friction polarity (Mi et al. 2018a). Nie used triethoxy-1H, 1H, 2H, 2H-tridecafluoro-N-octylsilane (PFOTES) to modify the surface of CNF, so that the output current of the PFOTES-CNF-based TENG was approximately twice that of the CNF-based TENG (Nie et al. 2021). Adding filler in the papermaking process could increase the contact area between the paper and another electrode owing to the existence of the filler, thus improving the performance of the TENG (Cuncun et al. 2019; Mi et al. 2018b). Ding used a porous polydimethylsiloxane (PDMS) film doped with carbon nanotubes (CNTs) and aluminum sheets as electrodes to assemble TENG. The output voltage was reported to be 16 times that of TENG using a PDMS film (Xiaoheng et al. 2018).

In this study, ethylenediamine (EDA) was used to modify the molecular surface of cellulose fibers, and an amino group with electron-donating ability was introduced into the cellulose fibers to improve the charge density on the surface of cellulose fibers. The modification of cellulose fibers could be characterized by techniques such as Fourier-transform infrared spectroscopy (FTIR), X-ray diffraction (XRD), and X-ray photoelectron spectroscopy (XPS). To test the contact electrification performance of cellulose fibers, the modified cellulose fibers was made into paper (nano TiO2 particles were added as papermaking

filler), and TENG was then assembled with Fluorinated ethylene propylene (FEP) film and measured using an electrometer.

Experimental

Raw materials and reagents

The raw cellulose fibers used was eucalyptus cellulose (Nanning, China). Chemical reagents such as sodium hydroxide, epichlorohydrin (EPI), EDA, and sodium bicarbonate were all analytically pure and purchased from Tianjin Zhiyuan Chemical Reagent. TiO_2 nanoparticles were purchased from Beijing Deke Daojin Technology Co., Ltd. (Beijing, China). An acrylic board was purchased from Yafan Plastic Trading Co., Ltd. (Foshan, China), conductive double-sided tape was purchased from Jufu Technology Co., Ltd. (Shenzhen, China), and FEP film was purchased from Jiahe Plastic Technology Co., Ltd. (Taizhou, China).

Amino modification of cellulose fibers

Ethylenediamine was not easy to replace with cellulose fibers fibers under mild conditions. Therefore, a two-step method was used to introduce amino groups into cellulose fibers. As shown in Fig. 1, epichlorohydrin was used to replace cellulose fibers, and then ethylenediamine reacted with epichlorohydrin, so as to introduce amino groups into cellulose fibers. First, 1 g of cellulose fibers was weighed and transferred into a 100 mL conical flask. Then, 50 mL of 0.1 mol/l NaOH solution and 5 mL epichlorohydrin were added and stirred in a constant temperature water bath (50 ℃) at 160 r/min for 6 h. After the reaction, the product obtained was epoxidized cellulose fibers (EPI cellulose). Subsequently, 1 g of EPI-cellulose fibers was weighed and transferred to a 500 mL conical flask. Next, 200 mL of ethylenediamine solution, with a volume concentration of 25%, and 3 g NaHCO₃ were added, and the reaction was oscillated in a constant temperature water bath at 75 ℃ for 7 h. After the reaction, the product obtained by suction filtration was an amino cellulose fibers (EDA-cellulose).

Preparation of paper and EDA-paper

A quantity of 0.6 g of cellulose and 0.6 g of EDA-cellulose (nano TiO_2 particles with a mass fraction of 0–30% as papermaking filler) were weighed and placed in a 500 mL conical flask. Then, distilled
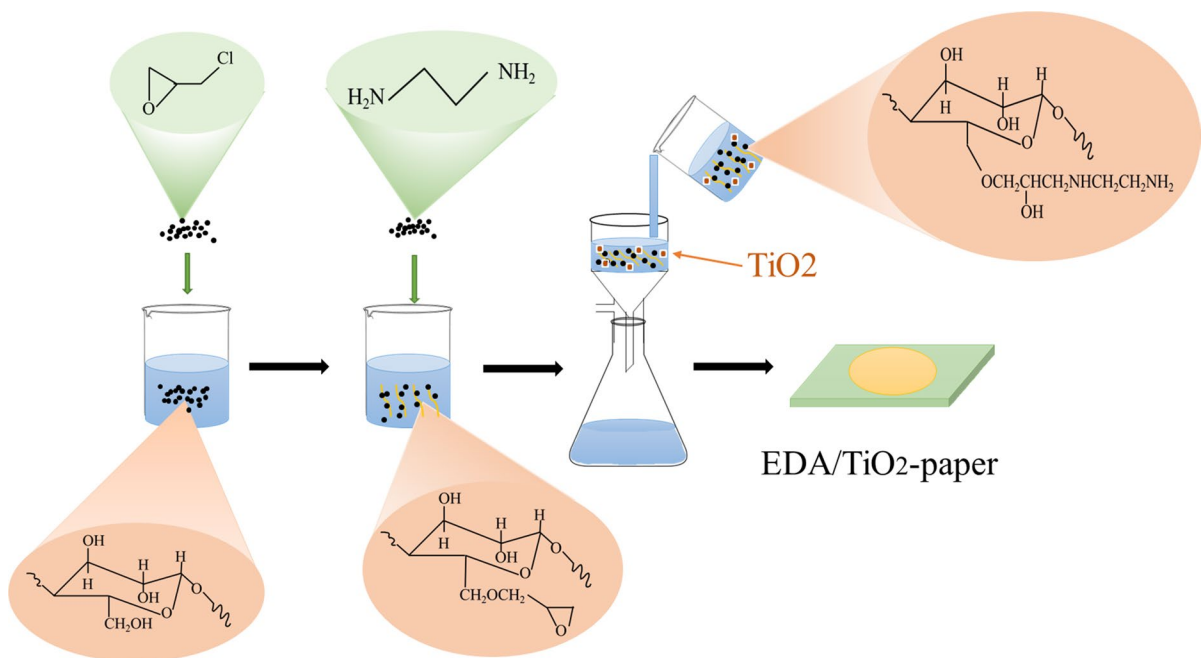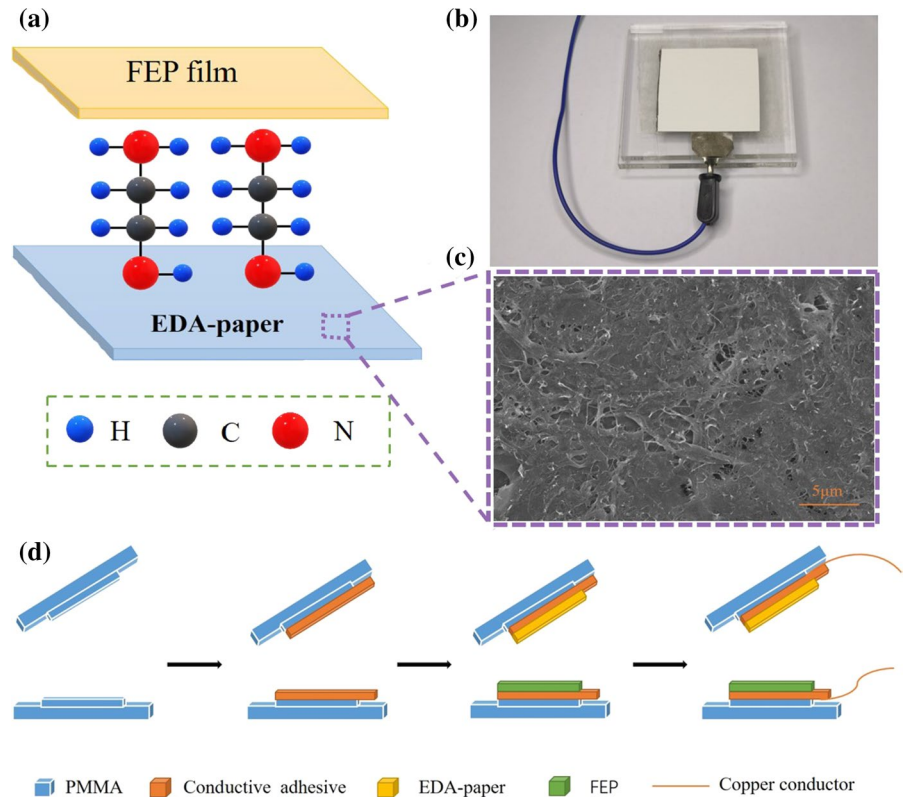

Fig. 1 Preparation process of EDA/TiO_2-paper

Fig. 2 **a** Schematic diagram of triboelectric nanogenerator (TENG) electrode; **b** Physical drawing of TENG electrode; **c** Scanning electron microscopy (SEM) image of EDA-paper; **d** TENG structure

water was added, the suspension was sonicated for 20 min, and then stirred at room temperature for 6 h to disperse the cellulose evenly. As shown in Fig. 1, the paper-making process used a more concise vacuum suction filtration method. The suspension with evenly dispersed cellulose fibers was poured into a G5 sand core funnel with a microporous filter membrane (Zhang et al. 2019b). After suction filtration, the paper was dried in an automatic molding dryer (ESTANITHAAGE BBS-2, Germany) at 75 °C for 15 min to obtain dry paper and EDA-paper.

Structure of TENG

As shown in Fig. 2, the TENG device was assembled based on a traditional vertical contact separation mode. A transparent acrylic plate was used as the supporting material for the device. The overall height of the acrylic plate was 5.8 mm, and the size was 7 cm × 7 cm. A raised structure in the middle of the plate measured 0.8 mm in height and 4 cm × 4 cm in size. Paper and EDA-paper were used as the anode electrode materials and FEP film was used as the

cathode electrode material. The electrode material was cut to a size of 4 cm × 4 cm, fixed on the acrylic plate with double-sided conductive tape, and a part of the conductive double-sided tape, on one side, was used to fix the copper conductor.

Characterization

Scanning electron microscopy (SEM) (Hitachi su8020, Japan) was used to observe the morphology and surface elemental distribution of cellulose fibers before and after amino modification. The diameter of cellulose fibers was calculated using the software "nano measurer 1.2". The samples were sprayed with gold prior to the observation. Atomic force microscopy (AFM) (Hitachi 5100n, Japan) was used to observe the roughness of the fiber surface. The tensile strength of paper was tested by universal material testing machine (WEB WBE-9809B, China). FTIR (Vertes 70, Germany) was used to analyze the changes in the molecular structure of cellulose fibers before and after amino modification. The scanning range of the test wave number was 4000–400 cm^{-1}.

XPS (Kratos Axis Ultra DLD, UK) was used to analyze the types and contents of the surface elements before and after cellulose fibers modification. XRD (Smartlab 3KW, Japan) was used to determine the change in the crystallinity of cellulose fibers before and after amino modification. The crystallinity (CRI) was calculated according to Segal method (Segal et al. 1959), and Eq. (1) was an empirical method for calculating cellulose crystallinity:

$$CrI(\%) = \frac{(I_{200} - I_{am})}{I_{200}} \times 100\% \qquad (1)$$

where I_{200} is the intensity of the diffraction peak at $2\theta = 22°$, I_{am} is the intensity of the diffraction intensity minimum at about $2\theta = 18°$.

Through a vibration exciter (jzk-10, China) and tubular linear motor (Linmot h10-70×240/210, US), the TENG was periodically subjected to a certain frequency and pressure. The generated electrical signal was captured using an electrometer (Keithley 6514, US) and an acquisition card (Ni usb-6259, USA).

Results and discussion

Characterization of cellulose fibers

FTIR could provide quantitative and semi-quantitative information, indicating the existence and absence of functional groups of lignocellulose before and after treatment. In addition, the change in peak strength could also indicate the change in functional group content. Figures 3a and b show the FTIR spectra at 4000–500 cm^{-1} and 1200–800 cm^{-1} before and after cellulose fibers modification. As shown in Fig. 3a, EPI—cellulose and EDA-cellulose retained the absorption peak of cellulose. After the cellulose fibers was treated with epichlorohydrin, a new functional group absorption peak appeared in the infrared spectrum of EPI-cellulose. As shown in Fig. 3b, the absorption peak at 1124 cm^{-1} corresponds to the antisymmetric stretching vibration of C–O–C, and the absorption peak at 1067 cm^{-1} is the symmetrical absorption peak of C–O–C (Muharam et al. 2017). The epoxy group originated from epichlorohydrin, indicating that the epoxy group was introduced into the cellulose fibers. After the EPI-cellulose was further treated with ethylenediamine, some new absorption peaks appeared in the infrared spectrum, of which the absorption peak at 1119 cm^{-1} is the stretching vibration peak of C-N, and the absorption peak at 830 cm^{-1} corresponds to the bending vibration peak of N–H. As shown in Fig. 3a, the absorption peak at 3168 cm^{-1} is the stretching vibration peak of N–H (Bo et al. 2009; Hattori et al. 2004), and these absorption peaks originate from the -NH$_2$ of ethylenediamine. This shows that amino groups were introduced into the cellulose fibers.
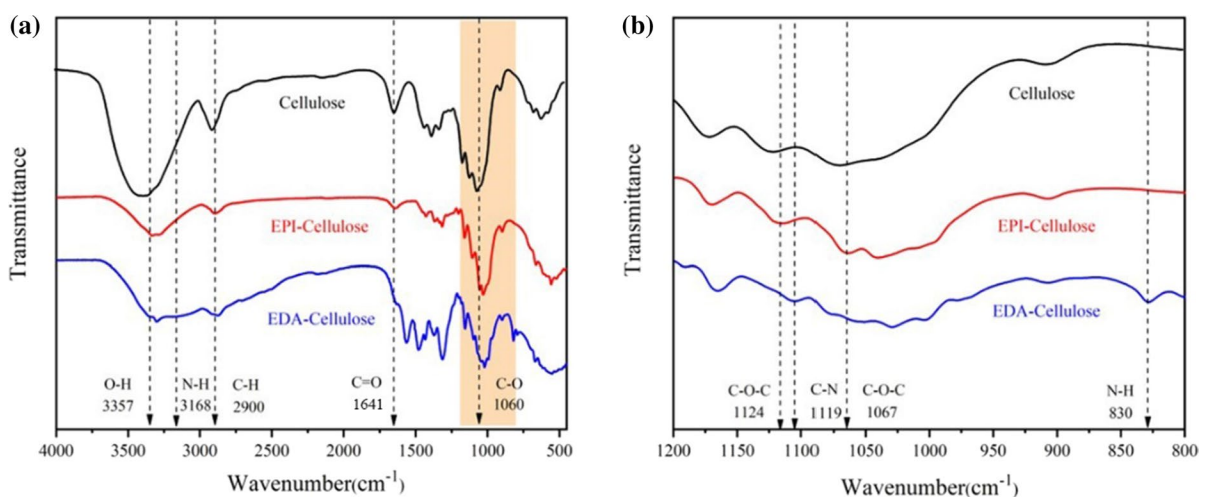

Fig. 3 Fourier-transform infrared spectroscopy (FTIR) spectra of cellulose fibers, EPI-cellulose and EDA-cellulose: a 4000–500 cm^{-1}; b 1200–800 cm^{-1}

XRD can be used to determine the changes in the cellulose structure, crystal form, and crystallization degree. As shown in Fig. 4, the peaks at $2\theta = 16°$, $22°$ and $34.5°$ are diffraction peaks of cellulose fibers in cellulose type I (French, 2014). The intensity of the
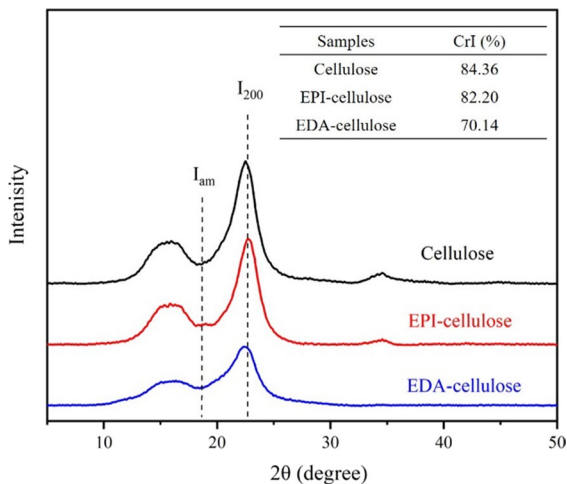
(200) peak for the EPI-cellulose decreased relative to that for the original material and further decreased for the ethylenediamine cellulose. Therefore, the CrI decreased from 84.4 to 82.2 to 70.1%. These can be attributed to the epoxy group on the surface of cellulose fibers being replaced by ethylenediamine, and the crystalline region of cellulose fibers being further destroyed, thus resulting in a decrease in crystallinity.

XPS can be used for quantitative and semi-quantitative analysis of the surface elements of the samples. As shown in Fig. 5a, the peaks of cellulose fibers and EPI-cellulose appeared at 532.4 eV and 286.5 eV, corresponding to O1s and C1s, respectively, and a new peak of EDA-cellulose appeared at 399.6 eV, corresponding to N1s. The proportion of elements on the sample surface analyzed by XPS is shown in Table 1. Compared with cellulose fibers, the C1s content of EDI-cellulose increased, and the O1s and O/C contents decreased. This was because epichlorohydrin was introduced into cellulose fibers, but epichlorohydrin introduced both C and O elements; hence, the proportion of elements on the sample surface changed slightly. N was detected on the surface of the EDA-cellulose. At the same time, the content of C1s
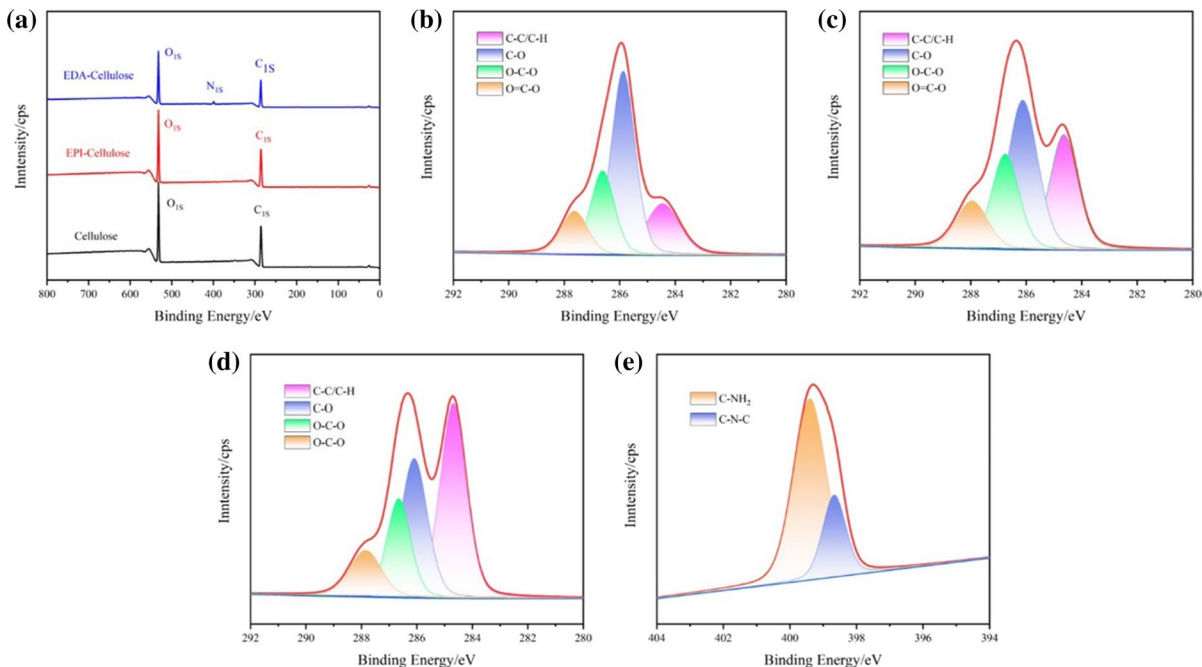

Fig. 4 X-ray diffraction (XRD) spectrum of cellulose fibers, EPI-cellulose and EDA-cellulose

Fig. 5 **a** Full spectrum of XPS before and after cellulose fibers modification; **b** C1s peak on cellulose fibers surface; **c** C1s peaks on EPI-cellulose surface; **e** C1s peaks on EDA-cellulose surface; **f** N1s peak splitting on EDA-cellulose surface

Table 1 Cellulose, EPI-cellulose and EDA-cellulose surface element ratio

Sample	C1s (%)	O1s (%)	N1s (%)	O/C (%)
Cellulose	55.72	44.28	0	79.47
EPI-Cellulose	56.18	43.82	0	77.96
EDA-Cellulose	60.85	37.19	1.96	61.09

continued to increase, and the contents of O1s and O/C continued to decrease. This was because ethylenediamine destroyed the epoxy group of epichlorohydrin, grafted to the sample surface, and introduced a large amount of C (Junka et al. 2014; Nie et al. 2020).

Surface topography

The SEM image of the cellulose fibers are shown in Fig. 6. Before modification, the cellulose fibers surface was smooth, without significant folds and a compact structure. After modification with epichlorohydrin and ethylenediamine, the cellulose fibers surface became rough, wrinkled, and loose. Simultaneously, the cellulose fibers began to break, and the specific surface area increased. This showed that after modification, the main chain of the cellulose fibers was destroyed, the chain length became shorter, and the amorphous region was degraded. At the same time, when the nano TiO_2 particle filler (with 5% mass fraction of EDA-cellulose in papermaking) was added, the distribution of nano TiO_2 particles could

be seen between the cellulose fibers. As shown in Fig. 7, the average diameter of cellulose was 9.63 μm and the average diameter of EDA-cellulose was 10.27 μm. There was little difference between the two. However, the diameter distribution of EDA-cellulose was relatively uniform, because part of EDA-cellulose was damaged to produce fine fibers, and some surfaces were wrinkled to increase the diameter of EDA-cellulose.

As shown in Fig. 8, the RMS value of paper after modification increased from 52.24 to 76.83 nm. After adding the nano TiO_2 particle filler, the RMS value of EDA-paper/5% TiO_2 further increased to 97.63 nm. The tensile stress of different kinds of paper is shown in Table 2. The tensile stress of EDA-paper reached 20.38 MPa, which was similar to that of A4 paper, indicating that EDA-paper had sufficient tensile strength for other aspects.

Output performance of TENG

The working principle of the vertical contact separation TENG is shown in Figs. 9a–d. In the initial state, electrodes I and II were in contact with each other. Because of the contact electrification effect, the electrons of electrode I were transferred to the surface of electrode II, such that the surface of electrode II was negatively charged and the surface of electrode I was positively charged. When the two electrodes were separated, a potential difference was generated, and electrons flowed from electrode II to electrode I, thus
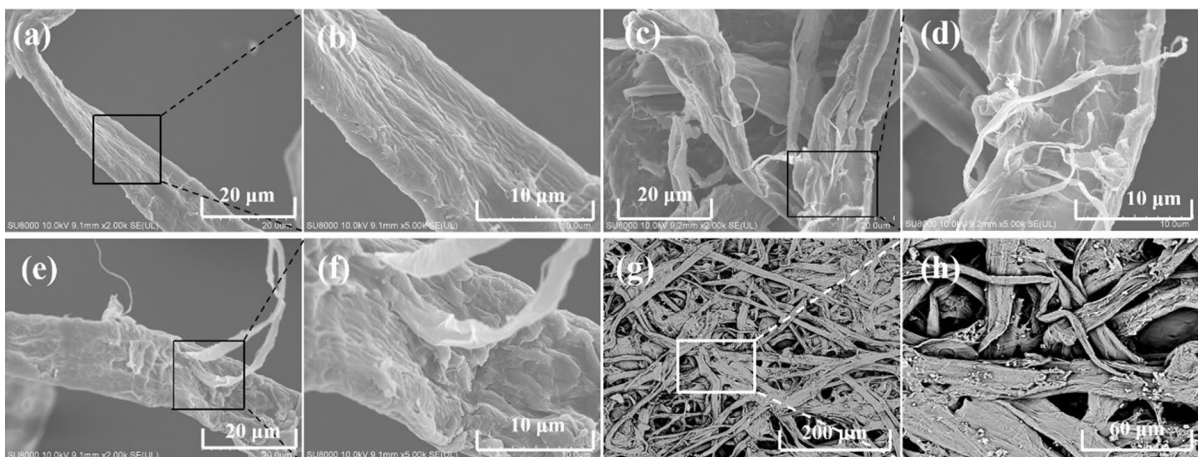

Fig. 6 SEM images at different magnification: **a** cellulose fibers×2000; **b** cellulose fibers×5000 **c** EPI-cellulose×2000; *d EPI-cellulose×5000 **e** EDA-cellulose×2000; **f** EDA-cellulose×5000 **g** EDA-paper/5% TiO_2×500; **h** EDA-paper/5% TiO_2×1000
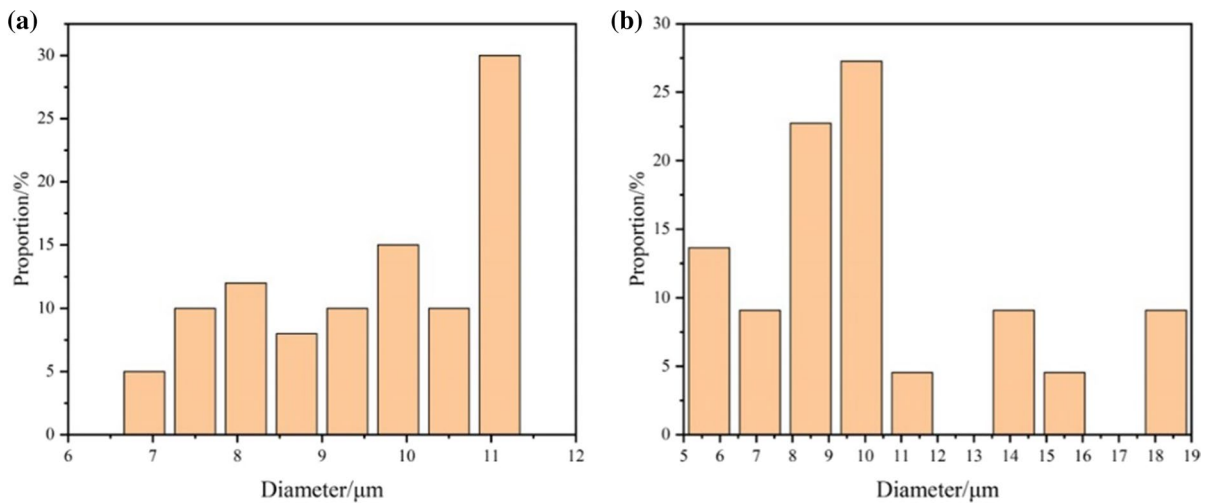
Fig. 7 **a** Cellulose fibers diameter distribution; **b** EDA-cellulose diameter distribution

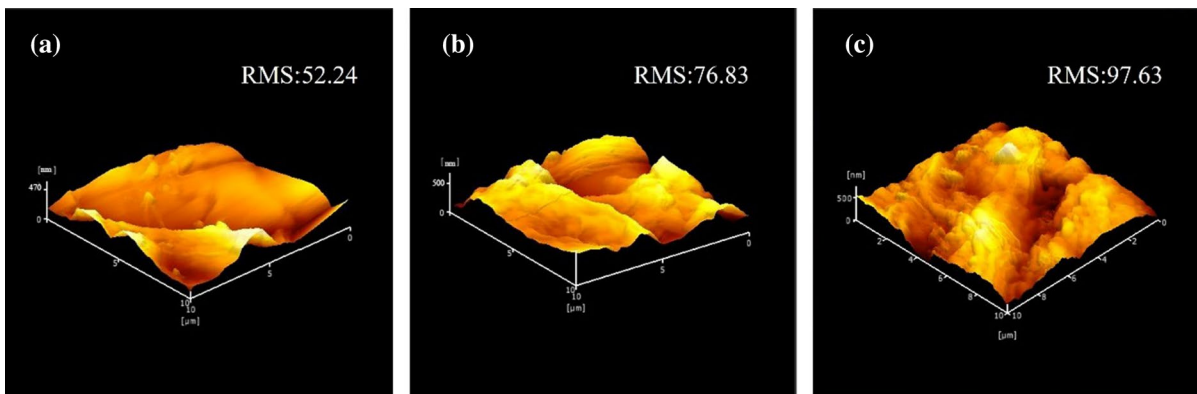**Fig. 8** AFM image (10 µm × 10 µm): **a** paper; **b** EDA-paper; **c** EDA-paper/5% TiO$_2$

Table 2 Tensile strength of paper

	Paper type		
	Cellulose fiber	EDA-paper	EDA-paper/5%TiO$_2$
Tensile stress (MPa)	12.15	20.38	9.36

generating a positive instantaneous current. When the electrode contacted again, the potential of electrode II would be higher than that of electrode I, and the electrons would move from electrode II to electrode I to produce a reverse instantaneous current. When the

two electrodes circulate for contact-separation movement, the TENG can carry out continuous electrical energy output (Mi et al. 2018a).

To explore the effect of amino modification on the contact electrification performance of cellulose fibers, paper-based TENG and EDA-paper-based TENG were used as experimental objects. In addition, the two electrodes of TENG were periodically contacted and separated by a linear motor, with an acceleration of 0.5 m/s^2 and a moving distance of 7 mm. As shown in Fig. 10, the open-circuit voltage of the paper-based TENG was 86 V and the short circuit current was 1.5 µA. The charge density was 1.8 nC cm^{-2}, the open circuit voltage of EDA-paper based TENG increased
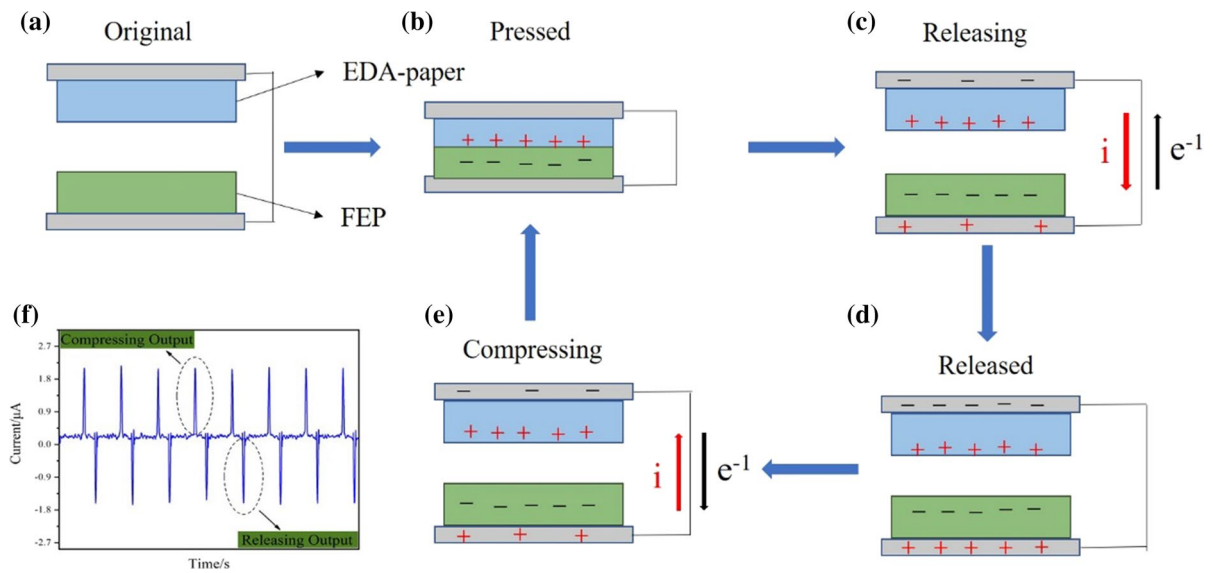
Fig. 9 Schematic diagram of working principle of contact separated TENG

from 86 to 116 V, by 34.9%, and the short circuit current increased from 1.5 to 1.9 µA, by 26.7%. The charge density increased from 1.8 to 2.1 nC cm^{-2}—an increase of 16.7%. This was because the amino group functioned as an electron source, which could improve the friction positive polarity of cellulose fibers and improve the electrical output performance of the TENG (Nie et al. 2021).

To explore the influence of the working frequency and contact pressure on the contact electrification performance of cellulose fibers, the EDA-paper-based TENG was used as the experimental object, and the working frequency of the TENG was controlled by a linear motor. As shown in Figs. 11a–c, when the acceleration of relative contact-separation

movement between two electrodes increased from 0.5 to 0.9 m/s^2, the open circuit voltage increased from 112 to 120 V (a 7.1% increase), and the closed-circuit current increased from 1.6 to 2.4 µA (a 50.0% increase). The charge density increased from 2.7 to 3.1 nC cm^{-2}, which translated to an increase of 14.8%. This was because, under the same contact pressure, a higher contact frequency could make the external electrons reach flow balance in a shorter time, shorten the duration of the current peak, and increase the short-circuit current (Shen et al. 2017). An exciter was used to control the contact pressure of the TENG. As shown in Figs. 11d–f, when the contact pressure between the two electrodes increased from 10 to 50 N, the open circuit voltage increased from
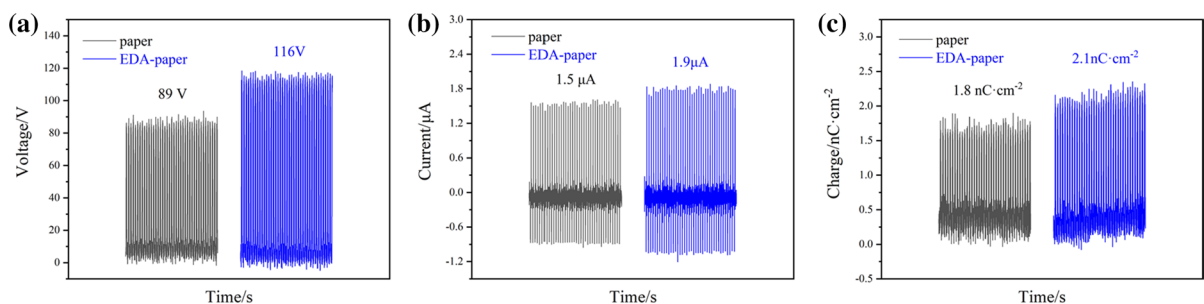

Fig. 10 Output performance of paper-based TENG before and after cellulose fibers modification **a** open circuit voltage; **b** closed-circuit current; **c** charge density
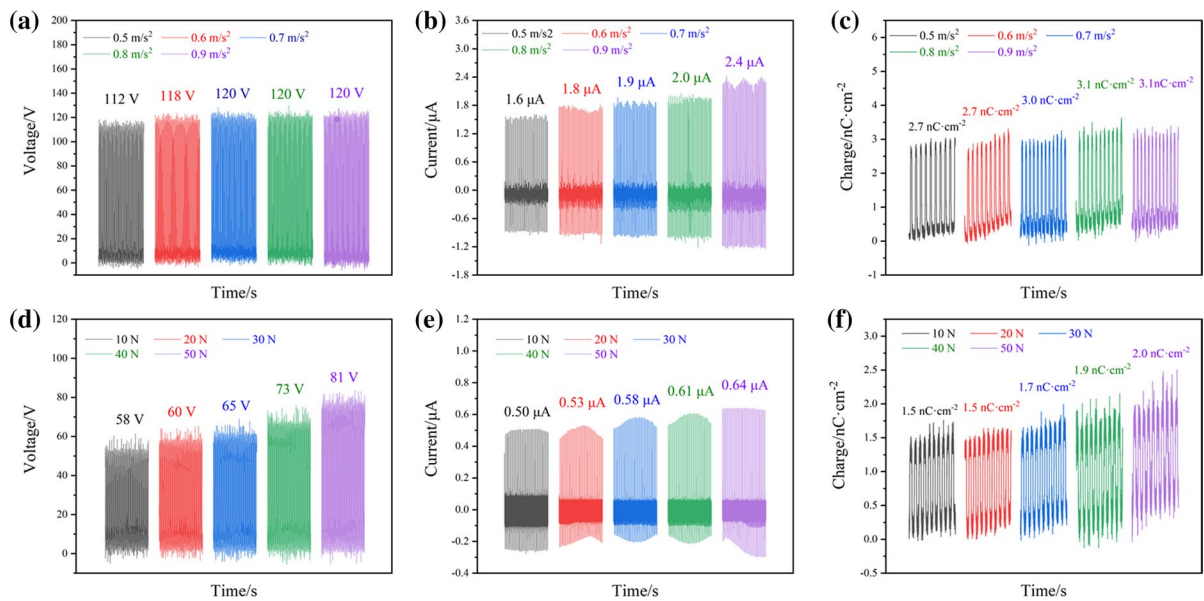
Fig. 11 **a–c** Open circuit voltage, short circuit current and charge density of TENG at different operating frequencies; **d–f** Open circuit voltage, short circuit current and charge density of TENG under different working pressures

58 to 81 V, which is an increase of 39.7%. In addition, the closed-circuit current increased from 0.50 to 0.64 μA (an increase of 28.0%), and the charge density also increased from 1.5 to 2.0 nC cm^{-2} (a 33.3% increase). This can be attributed to the surface of the EDA-paper being rougher. When the contact pressure was small, the rough surface prevented close contact with the FEP film. With the increase in contact pressure, EDA-paper deforms slightly and fills the gap with the FEP film, thereby increasing the contact area, and thus improving the output performance of the TENG (Zhang et al. 2019a; Zhu et al. 2013).

Used acrylic plates to splice into a transparent box, placed a hygrometer in the box, and sprayed water into the box with a watering can. When the air humidity in the box reached the target value (e.g. 60%) and was stable, put TENG into the box and stood for 2 h, and then took the value for test immediately. The movement acceleration between the two electrodes of the TENG was fixed at 0.5 m/s^2, and the influence of humidity on the contact electrification performance of cellulose fibers was studied by changing the ambient air humidity. As shown in Fig. 12a and b, with an increase in air humidity, the output performance of the TENG decreased to varying degrees regardless of whether the cellulose fibers was modified. When the air humidity increased from 60 to 90%, the open

circuit voltage of EDA-paper-based TENG decreased from 109 to 52 V, and the closed-circuit current decreased from 1.55 to 0.52 μA; they maintained levels of 47.7% and 33.6%, respectively. The output performance loss of the paper-based TENG was large. With the increase in air humidity, the open-circuit voltage decreased from 86 to 28 V, and the closed-circuit current decreased from 1.26 to 0.18 μA. They maintained levels of 32.6% and 14.3%, respectively. After introducing amino group into cellulose fibers, the surface energy of EDA-paper was reduced, the surface roughness became larger, the negative friction polarity of TENG was improved, and the influence of water vapor in air on the output performance of TENG was reduced.

Providing energy for external loads is the most common practical application of TENGs (Li et al. 2015; Mule et al. 2019). To explore the output performance of the EDA-paper-based TENG in the circuit, the TENG was connected to a variable resistance box, and its output performance in the range of 10^3–10^8 Ω was tested under the condition that the motion acceleration between the two electrodes was 0.5 m/s^2 and the motion distance was 7 mm. As can be observed from Fig. 12c and d, with the gradual increase in external resistance, the output voltage of TENG gradually increased, reaching a maximum value
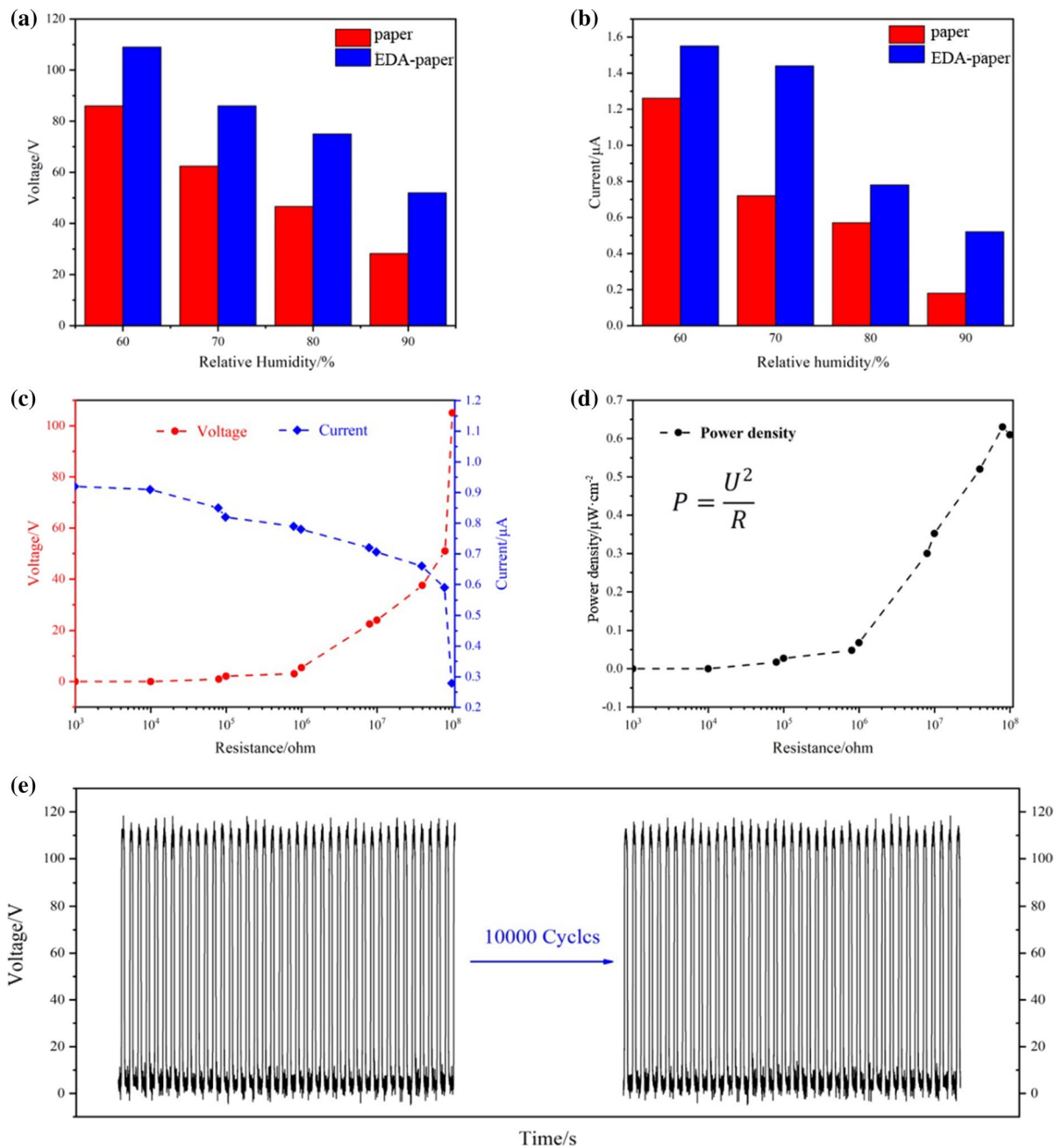
Fig. 12 **a–b** Changes of open circuit voltage and closed-circuit current of EDA-paper-based TENG with air humidity; **c** Change of output voltage and current of TENG under external resistance; **d** Power output curve of TENG under external resistance; **e** Continuous electrical output performance of TENG under 10,000 cycle contact-separation

of 105 V at a resistance of 10^8 Ω. Furthermore, the output current gradually decreased, and reached the minimum value of 0.28 μA at a resistance of 10^8 Ω. The output power increased first and then decreased at a resistance of 8×10^7 Ω, reaching a maximum

value of 0.63 μW cm^{-2}. With excellent output power, the EDA-paper-based TENG can be used to power small electronic devices. The output stability of the TENG is an important index for evaluating its practical application. The EDA-paper-based TENG was

tested under the condition that the motion acceleration was 0.5 m/s^2 and the motion distance was 7 mm between the two electrodes. The open-circuit voltage was tested after 10,000 continuous cycles. As shown in Fig. 12e, the open-circuit voltage in the beginning and end stages of the test was stable at approximately 115 V, thus indicating that the EDA-paper-based TENG was stable and reliable in providing long-term power for electronic devices.

TiO$_2$ could not only improve the roughness of paper and increased the contact area between electrodes, but also TiO$_2$, as one of the most commonly used papermaking fillers, did no harm to the environment and was an environmental protection material. Nano TiO$_2$ particles with different mass fractions were added to the paper to test its output performance. The test conditions were still that the motion acceleration between the two electrodes was 0.5 m/s^2 and the motion distance was 7 mm. It could be seen from Fig. 13a-c and Table 3 that when the mass fraction of nano TiO$_2$ particles was increased from 0 to 20%, the output performance of TENG was significantly improved. When the content of nano TiO$_2$ particles continued to increase to 30%, the open circuit voltage

and short circuit current of TENG did not increase, and the charge density only increased slightly. Considering the saving of materials, it was determined that the amount of nano TiO$_2$ added is 20% by mass. The corresponding open circuit voltage, closed-circuit current, and charge density were 147 V, 4.9 μA, and 4.0 nC cm^{-2}, respectively, which translate to increments of 26.7%, 157.9%, and 90.5%, respectively, compared to that before doping. The main reason was that after adding nano TiO$_2$ particles, some of them adhered to the surface of the paper. Under a certain pressure, the FEP surface would slightly

Table 3 Open circuit voltage, short circuit current and charge density of TENG with different content of nano TiO$_2$ particles

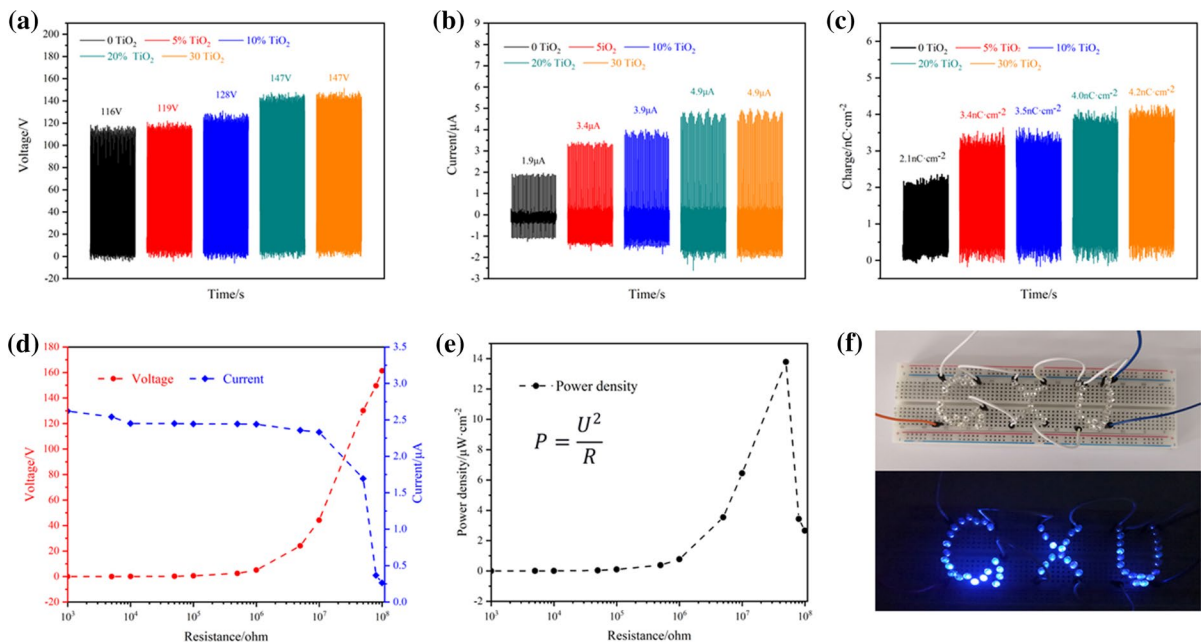| TiO$_2$ addition content (%)	Open circuit voltage (V)	Short circuit current (μA)	charge density (nC·cm^{-2})
0	116	1.9	2.1
5	119	3.4	3.4
10	128	3.9	3.5
20	147	4.9	4.0
30	147	4.9	4.2

Fig. 13 a–c: Open circuit voltage, closed-circuit current, and charge density of paper-based TENG doped with different mass fractions of TiO$_2$; **d–e**: The external resistance of EDA paper/20% TiO$_2$ based TENG is the change of voltage, current and instantaneous output power; **f** EDA -paper/20% TiO$_2$-based TENG lights up the LED bulb

deform to fill the space formed by nano TiO_2 particles, increase its contact area with the paper surface, and generate more surface charged during friction, thus improving the output performance of TENG. As shown in Fig. 11, the open circuit voltage, closed-circuit current, and charge density of EDA-paper/20% TiO_2-based TENG increased by 70.9%, 226.7%, and 122.2%, respectively, compared with paper-based TENG after amino modification and adding nano TiO_2 particles.

As shown in Fig. 13d and e, the TENG is connected to the resistance box. When the resistance increased from 10^3 to 10^8 Ω, the output voltage of TENG continued to increase, reaching the maximum value of 161 V at 10^8 Ω. In addition, the output current continued to decrease, and reached the minimum value of 0.26 μA at 10^8 Ω. The output power first increased and then decreased at a resistance of 5×10^7 Ω, reaching a maximum of 13.78 μW·cm^{-2}. Connect the shoes paper based TENG to the LED circuit board, as shown in Fig. 13f, more than 40 LED bulbs could be lit.

Conclusions

The cellulose fibers was treated with epichlorohydrin and ethylenediamine, and the amino group was introduced into the cellulose fibers. This not only changed the surface polarity of the cellulose fibers, but also made the fiber surface rougher, thereby improving the contact electrification performance of the cellulose fibers. When making paper, nano TiO_2 particles were added as filler to slightly deform the FEP film under a certain pressure. This increased the friction area between the paper and FEP film. The open-circuit voltage, closed-circuit current, and charge density of the EDA-paper/20% TiO_2-based TENG reached 147 V and the closed-circuit current reaches 4.9 μA. The charge density reached 4.0 nC cm^{-2}. When the resistance connected in the working circuit was 5×10^7 Ω, the output power reached 13.78 μW cm^{-2}. This shows that cellulose fibers have wide application prospects in the field of polymer replacement for TENG electrodes.

References

Bo M, Sun D, Zhu C, Liu C, Niu H (2009) Preparation of ethylenediamine chelating bacterial cellulose for the adsorption of copper ions. Ind Water Treat 29(7):60–62

Diaz AF, Felix-Navarro RM (2004) A semi-quantitative tribo-electric series for polymeric materials: the influence of chemical structure and properties. J Eletrostat 62(4):277–290

Fan FR, Lin L, Zhu G, Wu W, Zhang R, Wang ZL (2012) Transparent triboelectric nanogenerators and self-powered pressure sensors based on micropatterned plastic films. Nano Lett 12(6):3109–3114

French A (2014) Idealized powder diffraction patterns for cellulose polymorphs. Cellulose 21(2):885–896

Guo Y, Chen Y, Ma J, Zhu H, Cao X, Wang N, Wang ZL (2019) Harvesting wind energy: a hybridized design of pinwheel by coupling triboelectrification and electromagnetic induction effects. Nano Energy 60:641–648

Hattori K, Abe E, Yoshida T, Cuculo JA (2004) New solvents for cellulose. II. Ethylenediamine/thiocyanate salt system. Polym J 36(2):123–130

He X, Guo H, Yue X, Gao J, Xi Y, Hu C (2015) Improving energy conversion efficiency for triboelectric nanogenerator with capacitor structure by maximizing surface charge density. Nanoscale 7(5):1896–1903

Junka K, Filpponen I, Johansson LS, Kontturi E, Rojas OJ, Laine J (2014) A method for the heterogeneous modification of nanofibrillar cellulose in aqueous media. Carbohyd Polym 100:107–115

Lai SN, Chang CK, Yang CS, Su CW, Leu CM, Chu YH, Sha PW, Wu JM (2019) Ultrasensitivity of self-powered wireless triboelectric vibration sensor for operating in underwater environment based on surface functionalization of rice husks. Nano Energy 60:715–723

Li Y, Cheng G, Lin ZH, Yang J, Lin L, Wang ZL (2015) Single-electrode-based rotatory triboelectric nanogenerator and its applications as self-powered contact area and eccentric angle sensors. Nano Energy 11:323–332

Liu Y, Mo J, Fu Q, Lu Y, Nie S (2020) Enhancement of triboelectric charge density by chemical functionalization. Adv Funcy Mater 74:1–33

Ma M, Kang Z, Liao Q, Zhang Q, Gao F, Zhao X, Zhang Z, Zhang Y (2018) Development, applications, and future

directions of triboelectric nanogenerators. Nano Res 11(6):2951–2969

Mi HY, Jing X, Zheng Q, Fang L, Huang HX, Turng LS, Gong S (2018a) High-performance flexible triboelectric nanogenerator based on porous aerogels and electrospun nanofibers for energy harvesting and sensitive self-powered sensing. Nano Energy 48:327–336

Mi HY, Xin J, Cai Z, Liu Y, Turng LS, Gong S (2018b) Highly porous composite aerogel based triboelectric nanogenerators for high performance energy generation and versatile self-powered sensing. Nanoscale 10(48):23131–23140

Muharam S, Yuningsih LM, Sumitra MR. 2017. Characterization of superabsorbent hydrogel based on epichlorohydrin crosslink and carboxymethyl functionalization of cassava starch. In: American Institute of Physics Conference Series. pp. 1–8

Mule AR, Dudem B, Patnam H, Graham SA, Yu JS (2019) Wearable single-electrode mode triboelectric nanogenerator via conductive polymer-coated textiles for self-power electronics. ACS Sustain Chem Eng 7(19):16450–16458

Nie S, Cai C, Lin X, Zhang C, Wang S (2020) Chemically functionalized cellulose nanofibrils for improving triboelectric charge density of a triboelectric nanogenerator. ACS Sustain Chem Eng 8:18678–18685

Nie S, Fu Q, Lin X, Zhang C, Wang S (2021) Enhanced performance of a cellulose nanofibrils-based triboelectric nanogenerator by tuning the surface polarizability and hydrophobicity. Chem Eng J 404:1–9

Niu S, Wang ZL (2015) Theoretical systems of triboelectric nanogenerators. Nano Energy 14:161–192

Niu S, Wang S, Lin L, Liu Y, Zhou YS, Hu Y, Wang ZL (2013) Theoretical study of contact-mode triboelectric nanogenerators as an effective power source. Energ Environ Sci 6(12):3576–3583

Qian C, Li L, Gao M, Yang H, Cai Z (2019) All-printed 3D hierarchically structured cellulose aerogel based triboelectric nanogenerator for multi-functional sensors. Nano Energy 63:1–8

Roy D, Semsarilar M, Guthrie J, Perrier S (2009) Cellulose modification by polymer grafting: a review. ChemInform 38(7):2046–2064

Segal LC, Creely JJ, Martin AEJ, Conrad CM (1959) An empirical method for estimating the degree of crystallinity of native cellulose using the x-ray diffractometer. Text Res J 29(10):786–794

Shen J, Li Z, Yu J, Ding B (2017) Humidity-resisting triboelectric nanogenerator for high performance biomechanical energy harvesting. Nano Energy 40:282–288

Wang ZL, Wu W (2012) Nanotechnology-enabled energy harvesting for self-powered micro-/nanosystems. Angew Chem Int Ed Engl 51(47):11700–11721

Wang S, Zi Y, Yu SZ, Li S, Fan F, Long L, Zhong LW (2016) Molecular surface functionalization to enhance the power output of triboelectric nanogenerators. J Mater Chem A 4(10):3728–3734

Wu JM, Chang CK, Chang YT (2016) High-output current density of the triboelectric nanogenerator made from recycling rice husks. Nano Energy 19:39–47

Wu C, Wang AC, Ding W, Guo H, Wang ZL (2019) Triboelectric nanogenerator: a foundation of the energy for the new era. Adv Energy Mater 9(1):1–25

Xia K, Du C, Zhu Z, Wang R, Zhang H, Xu Z (2018) Sliding-mode triboelectric nanogenerator based on paper and as a self-powered velocity and force sensor. Appl Mater Today 13:190–197

Xiaoheng D, Hailin C, Xinghong Z, Mingyu L, Yuntian L (2018) Large scale triboelectric nanogenerator and self-powered flexible sensor for human sleep monitoring. Sensors 18(6):1713–1724

Yang W, Chen J, Zhu G, Yang J, Bai P, Su Y, Jing Q, Cao X, Wang ZL (2013) Harvesting energy from the natural vibration of human walking. ACS Nano 7(12):11317–11324

Yao CH, Yin X, Yu YH, Cai ZY, Wang XD (2017) Chemically functionalized natural cellulose materials for effective triboelectric nanogenerator development. Adv Funct Mater 27(30):1–7

Zhang L, Fei X, Du W, Han C, Chi Z, Wang Z (2014) Transparent paper-based triboelectric nanogenerator as a page mark and anti-theft sensor. Nano Res 7(8):1215–1223

Zhang C, Lin X, Zhang N, Lu Y, Nie S (2019a) Chemically functionalized cellulose nanofibrils-based gear-like triboelectric nanogenerator for energy harvesting and sensing. Nano Energy 66:104126–104136

Zhang N, Tao P, Lu Y, Nie S (2019b) Effect of lignin on the thermal stability of cellulose nanofibrils produced from bagasse pulp. Cellulose 26(13–14):7823–7835

Zhao K, Wang ZL, Yang Y (2016) Self-powered wireless smart sensor node enabled by an ultrastable, highly efficient, and superhydrophobic-surface-based triboelectric nanogenerator. ACS Nano 10(9):9044–9052

Zhu G, Lin ZH, Jing Q, Bai P, Pan C, Yang Y, Zhou Y, Wang ZL (2013) Toward large-scale energy harvesting by a nanoparticle-enhanced triboelectric nanogenerator. Nano Lett Lett 13(2):847–853

Zhu Y, Yang B, Liu J, Wang X, Wang L, Chen X, Yang C (2016) A flexible and biocompatible triboelectric nanogenerator with tunable internal resistance for powering wearable devices. Sci Rep 6:22233–22243

Zi Y, Jie W, Wang S, Li S, Zhong LW (2016) Effective energy storage from a triboelectric nanogenerator. Nat Commun 7(1):10987–10985